Sea ice growth in the eastern Weddell Sea in winter

C. Kottmeier, K. Frey,[1] M. Hasel, and O. Eisen[2]

Institut für Meteorologie und Klimaforschung, Universität Karlsruhe/Forschungszentrum Karlsruhe, Germany

Received 5 August 2001; revised 5 April 2002; accepted 21 February 2003; published 25 April 2003.

[1] The energy budget and the formation of sea ice in the eastern Weddell Sea west of Maud Rise are investigated on a regional scale on the basis of data obtained from drifting buoys deployed during the ANZFLUX project in 1994. A one-dimensional model for snow-covered sea ice and a kinematic-thermodynamic sea ice model for ice formed in leads are coupled and run under atmospheric and oceanic conditions specified from in situ data. Flooding at the snow-ice interface and snow ice formation need to be accounted for to achieve reasonable agreement between modeled and measured temperature distributions. The time-averaged values for the net heat flux are 21 W m^{-2}, some 60% of which originate in refreezing leads, and 9.8 cm for the monthly rate of ice accumulation. Whereas leads contribute a net accumulation of 10.8 cm, the mass balance of consolidated, snow-covered ice results in a net ablation of −1.0 cm. Sensitivity studies reveal the contribution of processes related to snow cover and ocean heat flux to sea ice formation and heat exchange. Without taking snow ice formation into account, a net ablation of −14.9 cm occurs under snow-covered ice due to high oceanic heat fluxes. A comparison between a simple two-layer model and the one-dimensional thermodynamic model emphasizes the influence of heat storage in sea ice on the development of heat flux and ice thickness. The heat and mass fluxes obtained on a regional scale, and their sensitivity to the parameterizations, elucidate the implication of vigorous small-scale processes on sea ice development and point out their importance for sea ice models. *INDEX TERMS:* 3394 Meteorology and Atmospheric Dynamics: Instruments and techniques; 1724 History of Geophysics: Ocean sciences; 3349 Meteorology and Atmospheric Dynamics: Polar meteorology; 4540 Oceanography: Physical: Ice mechanics and air/sea/ice exchange processes; *KEYWORDS:* sea ice, polynyas, air-sea-ice interaction, Weddell Sea, ANZFLUX, flooding

Citation: Kottmeier, C., K. Frey, M. Hasel, and O. Eisen, Sea ice growth in the eastern Weddell Sea in winter, *J. Geophys. Res.*, *108*(C4), 3125, doi:10.1029/2001JC001087, 2003.

1. Introduction

[2] The occurrence of large offshore polynyas in the Weddell Sea [*Zwally et al.*, 1983] during the winters of 1974–1976, i.e., the "Weddell Polynya," has given rise to various hypotheses attempting to explain an area of ~300,000 km^2 between 64°S and 69°S near the Greenwich meridian, where the ice concentration did not exceed 15%, while the surrounding area was covered nearly completely with ice. The explanations given for the existence of a large and persistent polynya disproved simple atmospheric reasons [*Martinson et al.*, 1981], though wind-driven ice divergence may initiate its formation [*Parkinson*, 1983]. It is very probable that the phenomenon is strongly related to more complex oceanic processes and coupled oceanic and atmospheric processes instead. In particular, *Gordon* [1981] proposed high oceanic heat fluxes to explain observations of a rather thin ice cover in 1981, supported by a simple polynya model study of *Martinson et al.* [1981] and oxygen measurements of *Gordon et al.* [1984]. Continuous remote sensing observations [*Gloersen et al.*, 1992] and different types of numerical studies [e.g., *Lemke*, 1987; *Timmermann et al.*, 1999; *Holland*, 2001; *Martinson*, 1990; *Beckmann et al.*, 2001] revealed new insights into such coupled processes occurring during the formation and conservation of the phenomenon.

[3] In the austral winter of 1994, the Antarctic Zone Flux experiment (ANZFLUX) was conducted partly to remedy a lack of in situ data from the Maud Rise seamount region (Figure 1), which are needed for studies of both small-scale and meso-scale processes in the sea ice and mixed layer, and for acquiring data suitable for testing model concepts for such processes [*McPhee et al.*, 1996]. The field program comprised two short manned ice drift station experiments as well as the deployment of automatic data buoys providing season-long records of mean ice motion, differential kinematic properties of ice motion (vorticity, divergence, shear), air temperature, air pressure and horizontal pressure gradients, high-resolution temperature profiles in

[1]Deceased 24 March 2002.

[2]Now at Alfred Wegener Institut for Polar and Marine Research, Bremerhaven, Germany.

0148-0227/03/2001JC001087$09.00

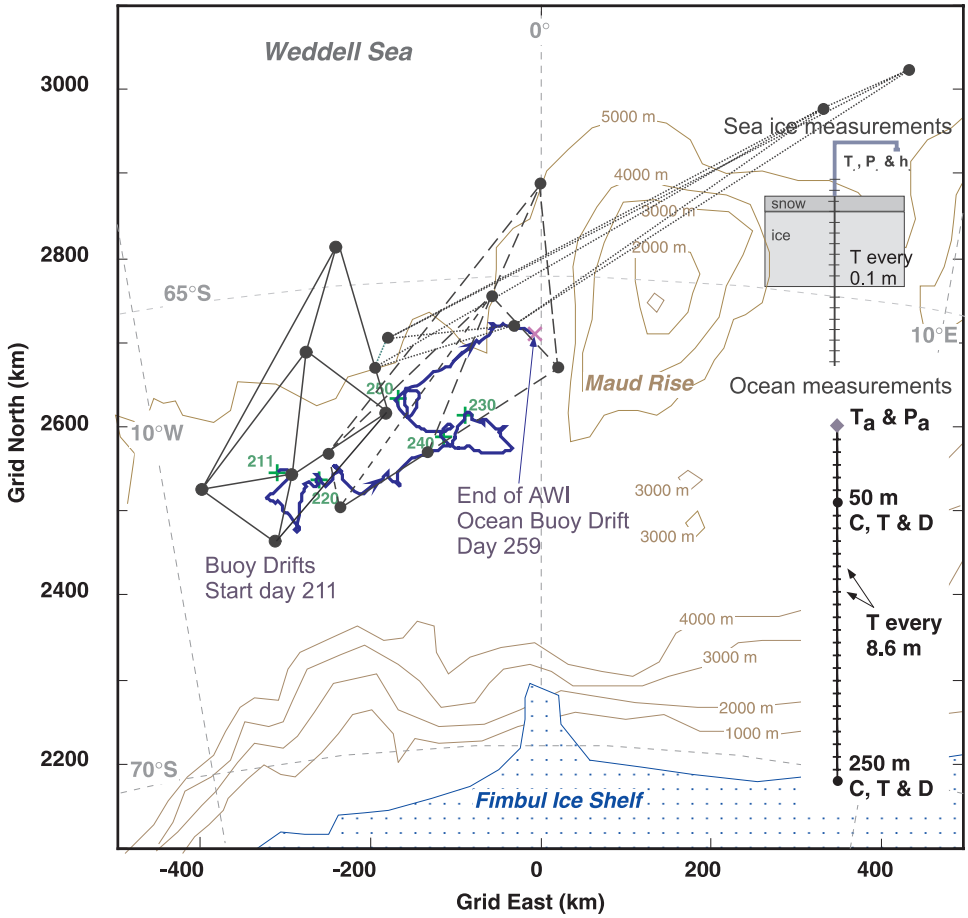

Figure 1. Drift track of the AWI buoys within the ANZFLUX buoy cluster. The buoys were deployed between 20 and 30 July, 1994, around the ANZFLUX Warm Drift camp. The track of buoy 9364 with thermistor strings in the sea ice and mixed layer is shown in blue. The sensor configuration is shown in the small figures on the right. Buoy locations on 1 August, 1 September, and 1 October are connected by solid, dashed, and dotted lines, respectively.

the ice cover, as well as mixed layer temperatures and salinities at various depths [*McPhee et al.*, 1999; *Kottmeier et al.*, 1997].

[4] Since its successful field phase in 1994, the availability of the unique ANZFLUX data sets stimulates analyses of relevant processes. Oceanic heat fluxes have been derived from turbulence measurements in the mixed layer during the manned ice-drift stations as well as from ice thermistor data [*McPhee et al.*, 1999]. Rather large mean ocean heat fluxes of 53 W m^{-2} for the region west of Maud Rise, of 23 W m^{-2} over Maud Rise, and of 27 W m^{-2} for the 44-day ice thermistor record, proved that the ocean heat flux may critically affect sea ice growth and melting in this region. The impact of regional oceanic conditions on heat fluxes for the ANZFLUX region has recently been studied by *Muench et al.* [2001] with two further approaches. Based on ship CTD and buoy data, they estimated the temperature excess above freezing point at a depth of 10 m. Alternatively, considering the interaction between Weddell Deep Water and the upper mixed layer, they calculated the averaged heat fluxes from dissolved oxygen (DO) and δ^3He measurements. Both methods agree in comparably large heat fluxes in the region west of Maud Rise. The results differ somewhat from those of *McPhee et al.* [1999], partly reflecting regional differences, but also because of the impact of different averaging as well as sampling characteristics. Based on a large number of oceanic measurements in the Weddell Sea, *Martinson* [1998] provided spatial distributions of bulk properties and they derived winter heat fluxes documenting the role of large heat fluxes in the Maud Rise region in reducing ice thickness.

[5] This paper focuses on the consequences of large oceanic heat fluxes and snow cover related processes on a regional scale of ~30,000 km^2. We aim at quantifying the components of the energy budget and mass balance of sea ice by combining models for thick snow-covered sea ice and for ice growth in leads, both forced by measured data. The one-dimensional sea ice model, being based on pioneering work of *Maykut and Untersteiner* [1971], considers heat transfer through snow-covered older ice floes as well as snow ice formation. A model for ice growth in leads [*Eisen and Kottmeier*, 2000] accounts for the fraction of leads within the area defined by the polygon of buoy positions and the highly variable energy exchange in leads [*Smith et al.*, 1990; *Maykut*, 1982]. Both models are matched with adequate ANZFLUX data from the automatic buoys for a 6-week winter period. The forcing data are prescribed on the basis of in situ observations; free parameters of the thermo-

dynamic model for snow-covered sea ice are specified by comparison with temperature measurements.

[6] The sensitivities of the spatial and temporal averaged ice formation rates and the energy balances to specific processes, namely the large oceanic flux, the insulating effect of a snow cover, and the flooding of sea ice, are examined by modifying the optimized models and forcing data. The implications of the sensitivity studies are complemented by results on the influence of the physical representation of heat storage in sea ice. Instead of a complex numerical sea ice component, large-scale models often use a two-layer thermodynamic formulation for snow-covered sea ice, resulting in simple linear vertical temperature distributions in snow and ice. As a consequence they fail to account for heat storage in the ice and snow slabs. A comparison of results of a simple two-layer model with the one-dimensional model provides further error estimates introduced by this simplified representation of physics.

2. Modeling Sea Ice Growth

[7] In the central and eastern Weddell Sea the main part of the sea ice cover consists of consolidated floes and refrozen leads. The frequent passage of low-pressure systems and related snowfall causes the thicker ice to be covered by a snow layer, which at many places becomes sufficiently thick to cause flooding at the ice-snow interface and formation of snow ice [*Eicken et al.*, 1995]. To estimate the heat fluxes and mass balance of the whole ice cover, we represent these two basic types of sea ice cover with different models.

2.1. The 1D Thermodynamical Model for Snow-Covered and Flooded Sea Ice

[8] A one-dimensional thermodynamical model, hereinafter referred to as M&U model, is used to represent the vertical transport of energy, the salinity distribution, as well as flooding and snow ice formation at the snow-ice interface. It is based on the thermodynamic models of *Maykut and Untersteiner* [1971] and *Maykut* [1978], the salinity model of *Cox and Weeks* [1988], and uses a physical description of flooding similar to *Eicken et al.* [1995]. The model yields the temperature distribution in snow and ice by solving the diffusion equations

$$(\rho c)_s \frac{\partial T_s}{\partial t} = k_s \frac{\partial^2 T_s}{\partial z^2} \tag{1}$$

in the snow and

$$(\rho c)_i \frac{\partial T_i}{\partial t} = k_i \frac{\partial^2 T_i}{\partial z^2} + \kappa_i I_0 e^{-\kappa_i z} \tag{2}$$

in the ice. In equations (1) and (2), $(\rho c)_{i,s}$ is the volumetric heat capacity, and $k_{i,s}$ the thermal conductivity; the indices, s and i, stand for snow and ice, respectively.

[9] According to *Untersteiner* [1961], $(\rho c)_i$ and k_i depend on the salinity of the ice S_i, whereas k_s changes with the density of the snow [*Sturm et al.*, 1997]. Since sea ice salinity affects thermal conductivity and temperature, but also varies with temperature, we account for salinity changes by coupled modeling of temperature and salinity changes. Sea ice salinity is related to the salinity S_b, density ρ_b and volume V_b of brine via $S_i = \frac{m_s}{M} = \left[\frac{V_b \rho_b}{M}\right] S_b$, where M is the total mass within a specified volume of sea ice. During cooling, ice formation at the walls of brine pockets reduces V_b, and S_i decreases since brine is squeezed out. Based on laboratory experiments, this process is parameterized by [*Cox and Weeks*, 1988],

$$\frac{dV_b}{dT} = -\frac{\rho_b V_b}{\rho_i S_b} \frac{dS_b}{dT} + V_b \beta_i, \tag{3}$$

where the thermal expansion (last term) is neglected in this context. Integrating between two temperatures T_1 and T_2 leads to

$$\frac{V_b(T_2)}{V_b(T_1)} = -\frac{S_b(T_1)}{S_b(T_2)} \exp\left[\frac{c}{1000\rho_i}\{S_b(T_1) - S_b(T_2)\}\right], \tag{4}$$

where $c = 0.8$ kg m^{-3} is the slope factor within the assumed linear relationship $\rho_b = 1 + cS_b$ between brine density and salinity, and the factor 1/1000 arises since salinity is given in parts per thousand. The required brine salinities for different temperatures are taken from empirical data [*Assur*, 1958], approximated by a third-order polynomial in temperature. Following *Eicken et al.* [1995], salinity changes of opposite sign are assumed during warming and thermal expansion of ice.

[10] Brine infiltration has been found to be an important process in field studies both in the Weddell Sea for the ANZFLUX experiment [*Rapley and Lytle*, 1998] and in the Amundsen and Ross Seas [*Jeffries et al.*, 1998]. Percolation may set in when ice permeability is sufficiently large [*Golden et al.*, 1998]. A minimum threshold value for the occurrence of percolation is a brine volume concentration $C_{b,V}$ of 50 [*Cox and Weeks*, 1975]. At higher $C_{b,V}$-values, salinity decreases due to brine drainage. The colder the ice, the greater is the brine salinity and density. The vertical temperature gradient in the ice controls the brine density profile, being unstable under winter conditions when ice is colder at the top. A quantitative empirical estimate of the rate of salinity change as a function of temperature gradient and brine volume is obtained by *Cox and Weeks* [1975] from their experiments with growing sodium chloride ice as

$$\frac{\Delta S}{\Delta t} = 1.68 \cdot 10^{-5} \frac{\Delta T}{\Delta z} - 3.37 \cdot 10^{-4} V_b \frac{\Delta T}{\Delta z}. \tag{5}$$

The equation is applied for all model layers to obtain $S(z, t)$; however, layers above an impermeable layer are considered as impermeable.

[11] Time dependent modeling of temperature and salinity starts with initial profiles of brine volume and salinity according to *Eicken* [1992], assuming an S-shaped profile, which is approximated by a third-order polynom. Little is known about the typical timescale of salinity changes in response to temperature changes. We assume that salinity does not adjust to fast temperature changes and use temperatures in the equation above, which have been low-pass filtered with a cutoff period of 3 days. It turns out that the S shape of the salinity profile with larger gradients at the base and top of the ice is basically preserved while desalination progresses.

[12] The second term on the right-hand side of equation (2) accounts for the energy input into the ice by solar radiation, where I_0 is the flux of solar radiation penetrating the ice, and κ_i is the extinction coefficient of ice. This term is set to zero when snow is present. This simplification is considered uncritical, since solar radiation is generally small in winter and snow albedo is high. To solve equations (1) and (2), the temperatures at the upper and lower boundaries must be known. The temperature at the base of the ice is kept constant at the freezing point of sea water (T_b = 271.2 K). The difference between the conductive heat flux, F_c^b, associated with an energy flux into the ice under winter conditions, and the heat flux from the ocean, F_o,

$$F_m^b = F_c^b - F_o, \tag{6}$$

determines the accretion or ablation of ice at the bottom by

$$F_m^b = -\rho_i L_{f,i} \frac{d(h_s + H_i)}{dt}, \tag{7}$$

where ρ_i is the density of ice; $L_{f,i}$ is the volumetric heat of fusion of ice, set as $2.67 \cdot 10^8 J\, m^{-3}$.

[13] The temperature at the upper surface is determined by the energy balance equation,

$$F_m^0 = F_R + F_L + F_l + F_e + F_s + F_c, \tag{8}$$

where F_R is the balance of shortwave radiation; F_L is the flux of downwelling longwave radiation; F_l is the emitted longwave radiation; F_e and F_s are the turbulent atmospheric fluxes of latent and sensible heat, respectively; and F_c is the conductive heat flux in the snow or ice. The flux F_m^0 on the left-hand side of equation (8) accounts for surface melting when the temperature exceeds 273.15 K. As long as the surface temperature remains below the melting point, $F_m^0 = 0$. Fluxes toward the surface are counted as energy gain, i.e., >0, and the fluxes away from the surface as energy loss, i.e., <0.

[14] Only that part of the incoming solar radiation that is neither reflected from the surface nor penetrates the ice or snow contributes to the energy balance at the surface,

$$F_R = (1 - i_0)(1 - \alpha)F_r, \tag{9}$$

where α is the albedo of the surface, depending on the thickness of snow and ice [*Shine and Henderson-Sellers*, 1985]; i_0 is the fraction of incoming solar radiation, F_r, penetrating snow or ice, and depends on the percentage of cloud cover [*Grenfell and Maykut*, 1977].

[15] The fluxes of longwave radiation are described by the Stefan-Boltzmann law,

$$F_L = \epsilon_a \sigma T_a^4 \tag{10}$$

and

$$F_l = -\epsilon_0 \sigma T_0^4, \tag{11}$$

where $\sigma = 5.66 \cdot 10^{-8}$ W m^{-2} K^{-4} is the Stefan-Boltzmann constant; ϵ_a is the longwave emissivity of the air, which depends on the fractional cloud cover c as $\epsilon_a = 0.765 + 0.22\ c^3$ [*König-Langlo and Augstein*, 1994]; ϵ_0 is the longwave emissivity of snow or ice, and $T_{a,0}$ are the temperature of the air and the surface, respectively.

[16] According to *Maykut* [1978], the turbulent atmospheric fluxes are

$$F_e = \frac{0.622 \rho L C_e V_{10}}{p_0} \left[A\left(f T_a^4 - T_0^4\right) + B\left(f T_a^3 - T_0^3\right) + C\left(f T_a^2 - T_0^2\right) + D(f T_a - T_0) + E(f - 1) \right] \tag{12}$$

and

$$F_s = \rho c_p C_h V_{10} (T_a - T_0), \tag{13}$$

where ρ_a is the density, c_p is the specific heat at a constant pressure of air, L is the latent heat of vaporization, C_e and C_s are the coefficients of turbulent heat transfer [*Kondo*, 1975], V_{10} is the wind speed 10 m above ground, p_0 is the air pressure at ground level, and f is the relative humidity. The constants have values of $A = 2.7798 \cdot 10^{-6}$ hPa K^{-4}, $B = -2.6913 \cdot 10^{-3}$ hPa K^{-3}, $C = 0.97920$ hPa K^{-2}, $D = -158.64$ hPa K^{-1}, and $E = 9653.2$ hPa. The conductive heat flux at the surface is described by [*Maykut and Untersteiner*, 1969],

$$F_c = \frac{k_s}{(1 + \zeta)\Delta z} \left(T_{(1,t'+\Delta t)} - (1 - \zeta) T_{(2,t')} + \zeta T_{(3,t')} \right), \tag{14}$$

with

$$\zeta = \frac{k_s \Delta t}{(\rho c)_s \Delta z^2}, \tag{15}$$

where Δz is the depth increment, and Δt = 1 h is the time step used by the model. $T(z, t)$ are the snow and ice temperatures at different depths and different times. Substitution of equations (9)–(14) into equation (8) yields an equation in which all quantities are either parameterized or available from measurements except for the surface temperature, T_0. It is obtained by an iterative process using the Newton-Raphson iterative method.

[17] Two modifications are applied to the basic version of the model to account for data prescription. The measured snow depth and the oceanic heat flux were highly variable during the ANZFLUX experiment. The snow cover increased from an initial value of 11 cm to more than 34 cm by the end of August. In early September, the snow depth decreased temporarily. As snow is an excellent insulator, the depth of the snow cover strongly influences the temperature distribution in the ice and thus may alter the net heat flux from the ocean to the atmosphere. Therefore, the model is run with a variable snow thickness instead of the constant value contained in its basic version. As the snow thickness is estimated from data, there is no need anymore to calculate the mass balance at the upper boundary.

[18] The second modification accounts for the measured values of the oceanic heat flux, originally one of the free parameters of the model. It is derived from oceanic data using a flux parameterization [*McPhee et al.*, 1999]. The

oceanic heat flux affects the ice thickness (see equation (6)) and, thus, the temperature distribution in the lower ice layers.

[19] The model accounts for snow ice formation in a simplified form based on the model of *Eicken et al.* [1995]. The freeboard height h_{fb} depends on snow and ice densities ρ_s and ρ_i, respectively, as well as thicknesses h_s and H_i, as

$$h_{fb} = H_i - \left(\frac{\rho_i H_i + \rho_s h_s}{\rho_w}\right). \quad (16)$$

Snow fall and melting at the base of the ice may cause the snow-ice interface to be depressed below the sea level and sea water may flood the ice. Field studies [*Jeffries et al.*, 1998] have shown that negative freeboard may not be sufficient to cause flooding, when permeability is too small. The model used here, however, assumes flooding to occur whenever h_{fb} results to be negative, as observed during the ANZFLUX cruise by *Rapley and Lytle* [1998], in East Antarctica by *Lytle et al.* [2000], and modeled by *Maksym and Jeffries* [2000]. The intruding water causes formation of a salty and warm slush layer at the base of the snow cover. The density of the slush is assumed as 1.5 ρ_s (estimated from data of *Eicken et al.* [1995]) and its initial temperature is the freezing temperature of sea water. Slush salinity results from the assumed mass fractions of snow (2/3) and water (1/3) and their salinities. The slush formation introduces a third layer (slush layer, index $_{sl}$), which alters the freeboard condition. The equation

$$h_{sl} = \frac{(\rho_i - \rho_w)H_i + \rho_s h_s}{\rho_W - \rho_m - \rho_s} \quad (17)$$

defines the equilibrium slush layer thickness h_{sl}. The transformation of the less dense slush layer to denser sea ice affects the freeboard conditions, which is accounted for by a follow-up of minor flooding events. Freezing of the slush layer is induced by heat conduction toward the colder adjacent snow and ice, associated with the release of latent heat of fusion due to partial freezing. Since the ice below the slush layer is only slightly colder initially, the downward heat conduction ceases after adjustment of temperatures. Freezing then proceeds by upward heat conduction in the snow layer until the total latent heat of fusion is removed, followed by a phase of cooling of the newly formed snow ice layer. The salt injected with the sea water into the slush layer is preserved until the slush is frozen. Afterward it alters the salinity profile due to gravity drainage.

2.2. Ice Growth in Leads

[20] Ice formation rates and salt release in winter depend sensitively on the presence of open and refrozen leads. The kinematic-thermodynamic sea ice model for leads, described in detail by *Eisen and Kottmeier* [2000], is used to determine the contribution of leads to the total heat and mass exchanges by open and snow-free refrozen leads as compared to the thicker snow-covered sea ice.

[21] The model is forced by data from the drifting buoys and from ECMWF analyses to simulate basic processes occurring in lead freezing for nine classes of snow-free thin ice with a thickness between 0 and 60 cm. The upper limit of each class is defined in Table 1. The energy balance model for thin ice, based on the model of *Maykut* [1978] as described above (equations (8)–(13)), is used for the thermodynamic component. The air temperatures and air pressure gradients derived from matching buoy data and ECMWF analyses, described later, are used to calculate the surface temperature iteratively from the energy balance equation for the ice surface. All heat fluxes at the surface are estimated at a time resolution of 6 hours for all nine classes of thin ice. The energy balance at the bottom of the ice, derived from the calculated conductive heat flux, and the measured oceanic heat flux [*McPhee et al.*, 1999], comparable to equation (6), determines the thermodynamic growth rate and, therefore, the ice thickness.

Table 1. Time-Averaged Distribution of Area, Net Heat Flux, and Mass Balance[a]

Ice/Snow Thickness, cm	Area, %	Net Heat Flux, W m^{-2}	%	Mass Balance, cm
Snow-Free Ice Formed in Leads				
0–1/0	<0.1	<0.1	0.00	0.7
0–3/0	0.6	0.8	3.9	1.9
0–5/0	0.8	1.3	6.3	3.0
0–7/0	1.2	1.9	9.4	3.8
0–10/0	2.1	3.2	15.5	5.0
0–15/0	3.5	4.9	23.8	6.4
0–20/0	4.7	6.1	29.5	7.4
0–40/0	11.8	10.7	51.9	9.9
0–60/0	15.6	12.7	61.7	10.8
Snow-Covered Ice Including Snow-Ice Formation				
~40/~25	84.4	7.9	38.3	−1.0
Total Area				
Weighted sum	100.0	20.6	100.0	9.8

[a]The percentage of the net heat flux is given as the fraction of the total net heat flux from ocean to atmosphere of 20.6 W m^{-2}. The mass balances are given as monthly averages and refer to the total area.

[22] The kinematic model part considers sea ice being two-dimensional and determines the area of newly opened or closed leads for each time step from the differential kinematic properties of sea ice motion as marked by buoys, i.e., combined arrays of three to seven instruments [*Kottmeier and Sellmann*, 1996]. Least square fitting the buoy drift vector $\mathbf{d} = (d_x, d_y)$ to a linear combination of the geographical position $\mathbf{r} = (x, y)$ of the form $\mathbf{d}(x, y) = \mathbf{U}r(x, y) + \mathbf{v}$ results in the components of the strain matrix $\mathbf{U}$ for each time step, from which the change in area can be determined. The development of the ice thickness distribution as a function of time is calculated by linking the thermodynamic to the kinematic components [*Eisen and Kottmeier*, 2000]. Positive divergence causes new leads to form, which then start to freeze over. In the case of negative divergence, the corresponding area is successively removed from the thinnest ice class present at a time. The ice classes interact by applying the thermodynamic growth rate for each ice thickness class at a given time to the area present in that class, and transferring volume from one class to another if the upper or lower ice thickness boundary, respectively, is reached. The time series of the total area, i.e., thin ice formed in leads and snow-covered thick ice, is shown in Figure 2.

2.3. Two-Layer Model

[23] In large-scale sea ice models, weather forecast models, and climate models, which include sea ice cover, fluxes

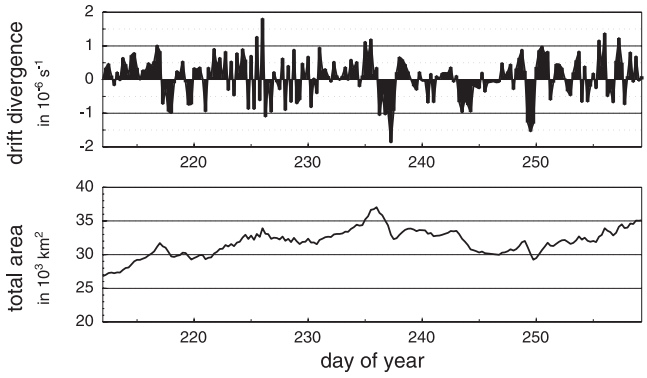

Figure 2. Response of total area to drift divergence as calculated by the lead model. Positive divergence forces the opening of leads and increases total area, negative divergence causes the thinnest ice to disappear and reduces the total area.

at the surface represent an essential boundary condition. Because of the required short calculation time, two-layer models are used to describe sea ice cover in these ocean-atmosphere models. However, they can only take into account one layer each of snow and ice. This leads to a greatly simplified description of the thermodynamical processes in snow and ice. In order to investigate the differences resulting from this simplification in comparison to the M&U model, we introduce a simple two-layer model similar to that described by *Semtner* [1976], which neglects heat storage.

[24] The two-layer model is forced by the same boundary conditions as the M&U model: The surface temperature at the upper boundary is calculated by solving the energy balance equation; the temperature at the base is constant. Unlike the M&U model, the two-layer model does not resolve the temperature profile within the ice or snow layer, but yields the temperature at the boundary between snow and ice as

$$T_{bd} = \frac{h_s H_i}{k_s H_i + k_i h_s}\left(\frac{k_s}{h_s}T_0 + \frac{k_i}{H_i}T_b\right). \qquad (18)$$

This concept is associated with a constant conductive heat flux that is proportional to the temperature difference between the base and the surface of the ice. Consequently, snow and ice lose their ability to store heat; the temperature wave at the surface penetrates the snow and ice layer immediately without any phase difference. This type of model is compared with more detailed 1-D models to study the net effect of it's simplifications on average energy fluxes and ice thickness.

2.4. Database for Model Forcing and Validation

[25] In the ANZFLUX experiment, six drifting buoys of the Alfred Wegener Institute (AWI) were deployed on the ice. They furnished readings of the air temperature, position, and air pressure, and transmitted this information every 3 hours via the ARGOS system. In equations (12) and (13), a combination of buoy measurements and ECMWF analyses yields horizontal pressure gradients [*Kottmeier and Sellmann*, 1996]; the wind at 10 m is assumed to be 70% of the geostrophic wind estimated from pressure gradients.

[26] One drifting buoy (buoy 9364, Figure 1) carried a 2-m-long thermistor string that had a sensor separation of 10 cm to measure temperature in snow and ice. The buoy transmitted data from 31 July to 16 September in the region displayed in Figure 1. When the buoy was deployed on the ice, the uppermost sensor was located some 70 cm above the ground, thus leaving the upper sensors above the surface, even when the snow thickness increased. In addition, it was also capable of measuring snow depth by means of an ultrasonic depth gauge installed 2.2 m above the ice, thus allowing the snow depth to be acquired continuously (Figure 3). The initial values for the snow depth, h_s, and the ice thickness, H_i, were 11 cm and 40 cm, respectively.

[27] The oceanic heat flux is determined from temperature measurements in the mixed layer by applying a bulk formula adjusted to turbulence flux measurements in the ocean boundary layer for the ANZFLUX "Warm Drift" [*McPhee et al.*, 1999] (Figure 3). In the course of the experiment, it varied between a maximum of 167 W m^{-2} and values lower than 3 W m^{-2} [*McPhee et al.*, 1999], with an areal average flux of 27 W m^{-2} over the first 76 days of the buoy drift.

2.5. Model Verification, Flooding Events, and Snow Ice Formation

[28] Model results are available for the operational period of the extensively equipped AWI-buoy 9364 from 31 July 1994 (day of year 211) to 16 September 1994 (day 259). We focus on two periods, lasting from 1 August (day 212) to 9 August (day 220), named period I, as well as from 29 August (day 230) to 18 September (day 250), named period II. Model results are compared with the buoy measurements, similar to a study by *Launiainen and Cheng* [1998] for the northern Baltic Sea. During the first period the buoy drifted from 66.9°S 6.8°E to 67.1°S 5.8°E. In this area, a manned drift station (referred to as the Warm Regime Station by *McPhee et al.* [1999]) was operational from 22 July until 29 July for the oceanic boundary layer studies. During the second period the buoy was west of Maud Rise between 66.7°S 1.1°E and 66.6°S 2.4°E. The model is initialized with a linear temperature profile in the snow and ice, and an ice thickness of 40 cm. It is first integrated

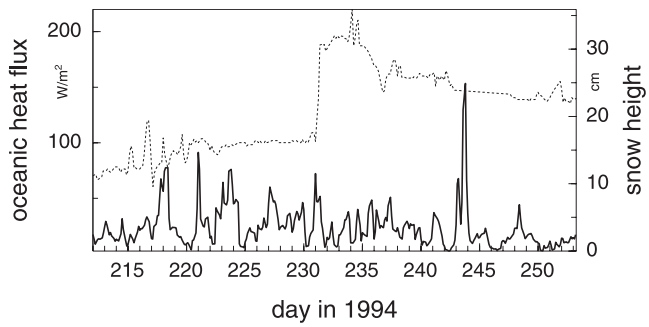

Figure 3. Time series of snow depth, measured with an ultrasonic depth gauge (dotted line), and ocean heat flux (solid line), determined from buoy temperature measurements in the mixed layer and ice drift data [*McPhee et al.*, 1999].

over 10 days to reach a near-equilibrium state, being based on a related study of *Frey* [1999] on the impact of changes of short-term forcing at 1-day period.

[29] The measured temperature distribution in snow and ice is shown in Figure 4a, and results of different model versions are shown in Figures 4b and 4c. In Figure 4b, the process of flooding is suppressed, whereas in Figure 4c this process is implemented as described above. The evolution of salinity in this case is shown in Figure 4d. In period I, the snow depth remains constant at ~12 cm and air temperatures varied between 244.0 K and 267.5 K. The model is rather close to the buoy measurements in both versions. This reflects that snow load and bottom melting are not sufficient to cause flooding. It also shows that model parameters, forcing data, parameterizations and numerical schemes result in a consistent description of the temporal evolution of sea ice temperature. Certain details, such as short-lived temperature changes, are smoothed out by the models, presumably caused by data noise and different vertical resolution of measured ice temperatures and model levels, at 10 cm and 5 cm intervals, respectively.

[30] Around the beginning of period II, the snow cover increases significantly. It is difficult to decide on the onset and amount of snowfall. An acoustic sensor mounted on the opposite side of the thermistor string through snow and sea ice proposes 15 cm of accumulation on day 231, being subject to uncertainty due to local effects. According to the thermistor chain measurements, one sensor originally in air became buried by snow on day 235. Observations during the ANZFLUX ship cruise, east of the buoy location, do not indicate precipitating weather systems at this time and we therefore attribute the effect to dislocation of previously fallen snow. Both snow depth proxies indicate consistently more snow after the events, respectively. We estimate snow depth as 20 cm until day 235 and as 30 cm from day 235 onward, though the change might have happened a few days before.

[31] The data indicate a rapid increase in temperature in the ice and in the lower part of the snow layer on day 237, which is not related to surface induced effects such as higher air temperatures (Figure 4a). Whereas the temperature gradient in the snow increases, the ice becomes almost isothermal. It is reasonable to assume that these changes are caused by flooding of seawater as a result of the previous snow accumulation. Three days later, on day 240, air temperature decreases, the slush layer is obviously frozen, and the ice cools down again.

[32] The model without flooding (Figure 4b) is not able to reproduce the measurements well in period II. At the time the measurements show an increase in ice temperatures, the modeled temperatures remain almost constant. About three days after the flooding event and throughout the remaining 20 days of the period, modeled temperatures remain higher than observed in the sea ice. This is caused by thermal insulation of the unmodified 30-cm-thick snow layer, by bottom melting, and by higher ice conductivity resulting from salinity evolution. The model version with flooding capability initiates flooding as a result of snow accumulation on day 235, followed by minor floodings as a result of successive adjustments to the equilibrium freeboard height as well as of bottom melting. It is closer to observations and reflects freezing of the slush layer within 3 days. Flooding causes an intrusion of warm and saline water, which markedly changes the vertical salinity and temperature structure and is noticeable for the rest of the period. The net result of both model runs over the whole period is a thinning of sea ice by −18 cm (−45% of initial ice thickness) by bottom melting without flooding, whereas ice thickness is almost balanced (−1 cm; −2.5%) with flooding, consisting of −9 cm bottom melting and +8 cm snow ice formation. The reduced bottom melting is mainly caused by a thinning of the snow cover, which intensifies the net heat transfer to the atmosphere in periods with frozen slush.

3. Regional Scale Energy and Mass Balance

[33] Evaluating the regional balance of heat fluxes, ice production, and related quantities requires knowledge of their distribution as a function of ice thickness and of the ice thickness distribution. To account for the effects of a nonlinear temperature gradient in thick ice and the presence of a snow cover, the net heat flux and ice production for snow-covered thick ice are calculated with the one-dimensional thermodynamical model, assuming flooding and snow ice formation whenever the freeboard h_{fb} is calculated to be negative. For thin ice, formed in refreezing leads, the same quantities are calculated with the kinematic-thermodynamic sea ice model, which assumes a linear temperature distribution and does not consider snow cover. The kinematic component of this model also provides the ice thickness distribution. Combining the area weighted results of both models allows the estimation of the net heat flux and ice production for an area covered with sea ice of different origins and thicknesses as well as varying spatial thickness distributions. The quantities for the different ice classes discussed below are first weighted by their area and then averaged over the 47-day period of observation.

[34] The contribution of different ice thickness classes to the net heat flux points out differences in the heat flux versus area ratio of thin ice formed in refreezing leads and older ice covered with snow. During the period of observation, some 84% of the ice surface are composed of consolidated snow-covered ice floes, which contribute 38% to the total net heat flux of 20.6 W m^{-2} (Table 1). Some 30% of the net heat flux originates from ice not thicker than 20 cm, occupying less than 5% of the area. The net ice formation of 9.8 cm per month solely occurs under ice formed in leads. Thick ice floes have an almost balanced mass balance of −1 cm per month, being made up of melting at the bottom and snow ice formation at the top. During the observational period, 3.8% of the ice originating from leads grew thicker than 40 cm. Even without snow fall, it is therefore probable that snow drifting from adjacent floes caused some snow accumulation on ice formed in leads. Since thinnest ice is less affected, the resulting effect of reduced heat losses and ice formation rates remains presumably small.

4. Sensitivity Studies

[35] Several atmospheric and oceanic processes interact in the formation of sea ice, altering the thickness distribution on a regional and local scale. We want to quantify the significance of some of the most obvious processes, which

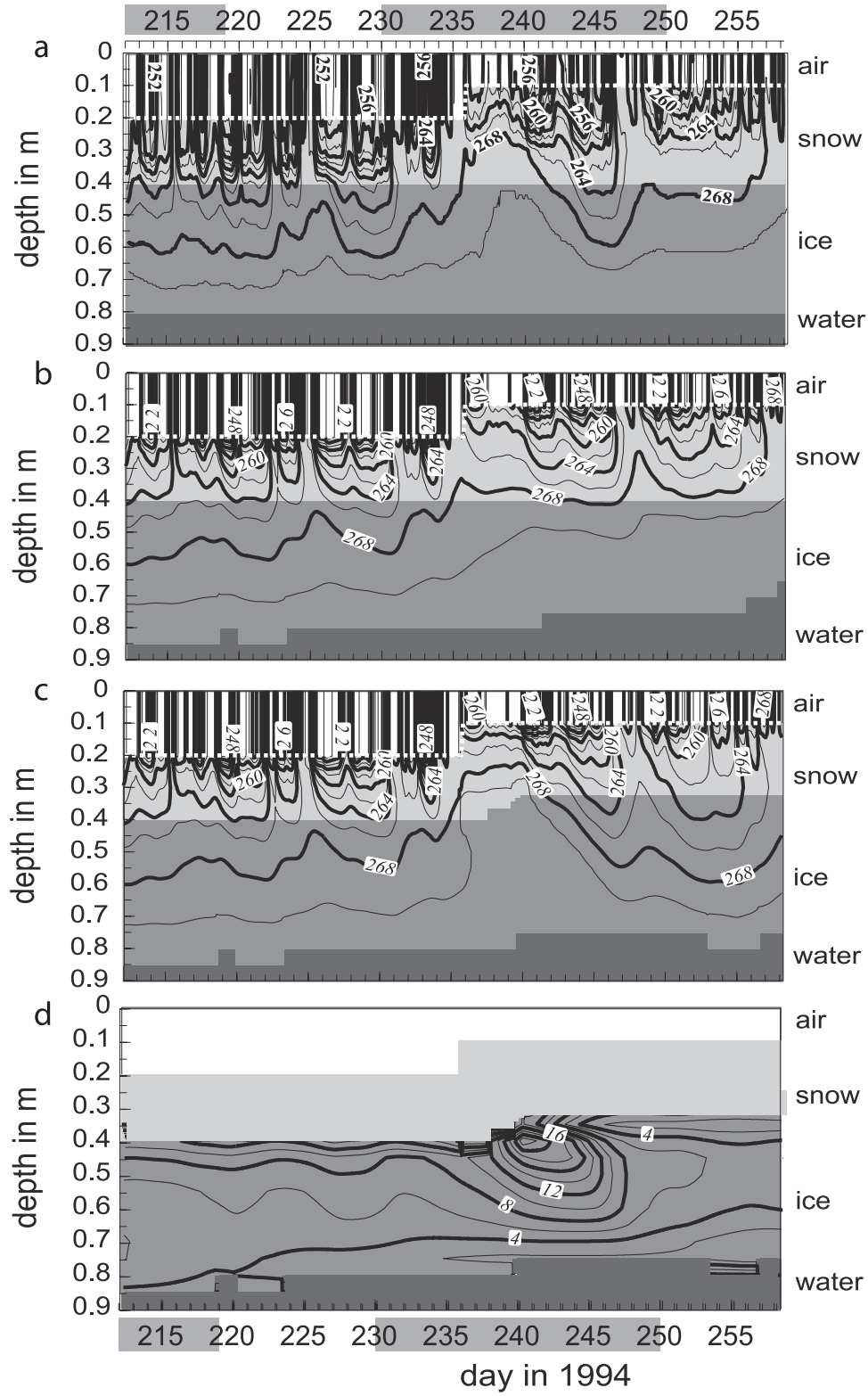

Figure 4. Comparison between the temporal evolution of the temperature distribution (temperatures in *K*) in the snow-covered ice slab: (a) measured temperatures, (b) modeled temperatures without flooding, (c) modeled temperatures with flooding on day 235 and subsequent snow ice formation, and (d) evolution of salinity (in parts per thousand) with flooding as in Figure 4c. The y axis denotes the depth in respect to uppermost sensor of the thermistor string. The margins between air, snow, ice, and water are plotted at the model resolution of 5 cm. Periods I and II are marked on x axes at the top and bottom.

are the oceanic heat flux, the snow ice formation, and the insulating effect of the snow cover, in three sensitivity experiments. Moreover, we investigate the influence of heat storage in a sea ice slab by comparing results from the standard model for thick ice (M&U) and the simple two-layer model (2L).

[36] As pointed out by earlier studies [e.g., *Martinson et al.*, 1981; *McPhee et al.*, 1996, 1999; *Muench et al.*, 2001], the rather thin sea ice cover in the Maud Rise region is usually attributed to large oceanic heat fluxes F_o. Oceanic heat supply determines ice growth at the bottom of the sea ice, and, by modification of ice thickness, indirectly affects heat fluxes at the ice surface. A lower oceanic heat flux results in enhanced ice production, thus intensifying the insulating effect of sea ice for the energy transfer from ocean to atmosphere.

[37] The influence of F_o on ice production and net heat flux of all ice thickness classes is investigated by comparing two model runs. The standard run, results of which were presented above, uses the oceanic heat flux time series estimated by *McPhee et al.* [1999] for the time from 31 July to 16 September 1994. Alternatively, we change the oceanic forcing by setting $F_o = 0$, with all other forcing data left unchanged.

[38] The averaged monthly ice production under classes of thin ice increases by 25%, from 10.8 cm in the standard run to 13.5 cm in the sensitivity run (Table 2), their overall areal percentage is slightly decreased by 3%. This is mainly due to the production of ice classes thicker than 20 cm (Figure 5) and the transfer from area of class 9 (40–60 cm) to the consolidated floe class. The ice formation of consolidated ice floes turns from a slightly negative to a strongly positive mass balance, resulting in a total ice production of some 36 cm, more than 3 times as much as in the standard run. The area-weighted net heat flux to the atmosphere through open and refrozen leads is reduced from 12.7 W m^{-2} in the standard run to 10.7 W m^{-2} in the sensitivity run, causing a decrease of the total net heat flux to 18.9 W m^{-2}. The area weighted net heat flux through snow-covered ice remains almost constant, resulting as 8.2 W m^{-2}.

Table 2. Time-Averaged Distribution of Area, Net Heat Flux, and Mass Balance for the Sensitivity Runs

Model	Area, %	Net Heat Flux, W m^{-2}	Mass Balance, cm
		Full Standard Model	
Leads	15.6	12.7	10.8
Thick ice	84.4	7.9	−1.0
Weighted sum	100.0	20.6	9.8
		No Oceanic Heat Flux	
Leads	12.9	10.7	13.5
Thick ice	87.1	8.2	22.6
Weighted sum	100.0	18.9	36.1
		No Snow-Ice Conversion	
Leads	15.6	12.7	10.8
Thick ice	84.6	8.1	−14.9
Weighted sum	100.0	20.8	−4.1
		No Snow Cover	
Leads	15.6	12.7	10.8
Thick ice	84.6	49.9	20.5
Weighted sum	100.0	62.6	31.3

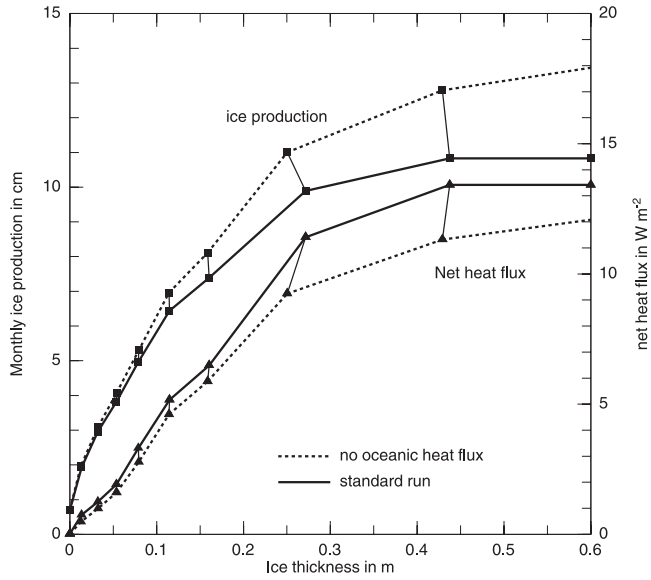

Figure 5. Influence of the oceanic heat flux on (top) ice production and (bottom) net heat flux in refreezing leads. The average thickness during the period of observation of each ice class is used as abscissa value. The ordinate values are area weighted, averaged over time, and cumulated in respect to ice thickness.

[39] The two opposing effects caused by the accumulation of snow on consolidated floes, i.e., reduced simple thermodynamic growth by larger insulation and increased mass balance by snow ice formation, are considered to be essential for the varying constitution of the sea ice cover [*Lange and Eicken*, 1991; *Eicken et al.*, 1994; *Worby et al.*, 1996]. In the second sensitivity experiment, snow ice formation is neglected, i.e., allowing a negative free-board without flooding. This causes a significant effect on the total mass balance. Whereas it was positive and controlled by ice production in refreezing leads (Table 1), it is now negative, and melting under thick floes (−14.9 cm) outweighs ice formation under thin ice (Table 2). The total ice production hence decreases from +9.8 to −4.1 cm. Despite this reduced mass balance of thick ice, the net heat flux is basically uninfluenced.

[40] In the third sensitivity run, both the insulating and weight effects of the snow cover are suppressed by setting $h_s = 0$ at all times, without changing any other forcing data. The net heat flux through thick ice increases sixfold, thus essentially tripling the total net heat flux to some 63 W m^{-2}. The accretion under thick ice turns from slightly negative to strongly positive, resulting in a total ice production of 31.3 cm, 3 times as much as in the standard run.

[41] In addition to the atmospheric (including snow) and oceanic forcing, the modeled temperature distribution in sea ice strongly depends on the model physics and vertical resolution. To provide an error estimate when heat storage in thick ice is neglected, we evaluate the differences between the two-layer model described in section 2.3 and the standard M&U model, using the identical forcing. As the 2L model neglects flooding, we use the results of the one-dimensional model without snow ice formation, as described for the second sensitivity study above, for com-

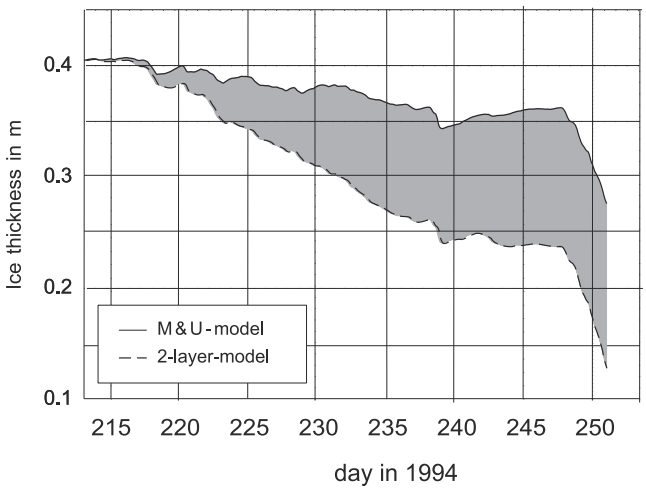

Figure 6. Ice thickness development over the whole period from 31 July to 16 September calculated by the M&U model and the two-layer model. The shaded area shows the difference between the two models.

parison of the development of ice thickness and energy balance for the period of observation.

[42] Starting with an initial ice thickness of 40 cm (Figure 6), both models predict an overall melting of the ice; between 12 and 16 September, especially, when high oceanic heat fluxes prevailed [*McPhee et al.*, 1999], ice thicknesses are strongly reduced. For 16 September, the M&U model without snow ice formation predicts an ice thickness of 27.6 cm, whereas the ice in the 2L model is only 12.3 cm thick. The temperature gradients are also larger than those of the linear temperature distribution of the 2L model (Figure 7). Despite similar forcing data and identical parameterizations of the atmospheric fluxes in both models, the instantaneous surface temperatures differ, and thus all temperature-dependent components of the energy balance differ. The mean surface temperatures, however, are 257.1 K and 256.9 K for the M&U and 2L model, respectively; this difference is just slightly smaller than the mean absolute difference of 0.3 K.

[43] The mean value of the constant conductive heat flux of the 2L model, $\bar{F}_c$ = 11.1 W m^{-2}, is almost equal to the mean conductive heat fluxes at the base and at the top of the M&U model, $\bar{F}_c^b$ = 11.5 W m^{-2} and $\bar{F}_c^{top}$ = 11.7 W m^{-2}, respectively. The mean absolute differences of the conductive heat fluxes at the base and at the upper surface of both models differ by 11.1 W m^{-2} and 4.2 W m^{-2}, respectively, and amount to some 96% and 36% of the mean conductive heat fluxes. This difference depends on the snow and ice temperature; they show better agreement when snow and ice warm up, as happens toward the end of winter, but the differences increase in periods of cooling (Figure 7).

5. Significance of Processes to Mass and Energy Balance

[44] In addition to the results of these rather rough sensitivity experiments, i.e., turning forcing and physical parameters just on and off, the comparison of the M&U model without snow ice formation and the 2L model yields a more detailed insight into the physics. The different temperature distributions of both models explain the observed discrepancies in ice thickness and heat flux. As the thermodynamic ice growth at the base depends on the difference between the conductive heat flux, F_c^b, and the oceanic heat flux, F_o, the temperature gradient in the lower ice layers is important for the ablation or accretion of ice at the bottom. Due to the larger temperature gradient of the M&U model, more heat is transported into upper layers of the ice, where it can be stored, leaving it unavailable for melting at the base of the flow; thus the M&U model yields a larger ice thickness than the 2L model.

[45] The excess of the mean conductive heat flux at the upper surface to that at the base by 0.25 W m^{-2} indicates warming of snow and ice during the modeled period. Comparison of the mean snow and ice temperatures on 31 July with those on 16 September correspond to warming of snow by some 6.0 K, and of ice by some 0.6 K. The change in the amount of heat stored in snow and ice is $\Delta Q_{s,i} = (\bar{\rho}c)_{s,i}\bar{V}_{s,i}\Delta T_{s,i}$, where $\bar{V}_{s,i}$ is the mean volume and $\Delta T_{s,i}$ is the temperature change in snow and ice, respectively. In these 47 days, $\Delta Q_{s,i}$ requires a total energy input of ΔF_{total} = 0.56 W m^{-2}, which is close to the value of 0.25 W m^{-2} caused by the different conductive heat fluxes at the upper surface and the base. Obviously, the M&U model provides a sound description of the heat storage, thus allowing the warming of snow and ice toward the melting season to be reproduced. Considering the differences of both models in terms of heat fluxes, the results do not differ significantly on a longer time scale, although the ice thicknesses show only a poor agreement.

[46] The contributions of the other three processes to ice production and heat exchange, calculated in the sensitivity runs, are evaluated by comparison with the results of the standard run. In the standard run, the highest ratio of heat flux to area percentage is found for ice up to 10 cm thick, indicating that despite their small contribution to area, these ice classes are nevertheless important for the total net heat flux. For the given ice thickness distribution, the ice refreezing in leads makes up the major component of the

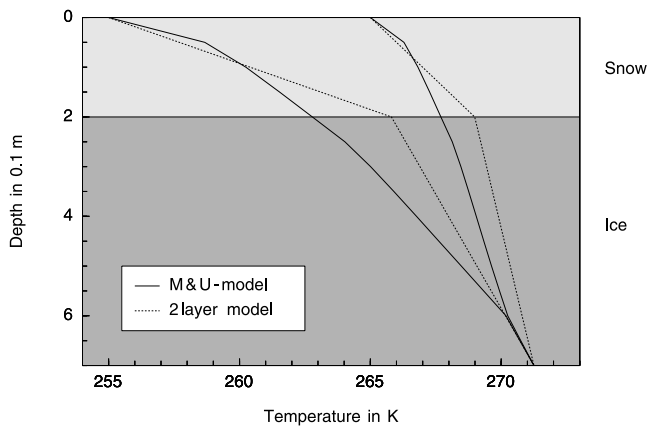

Figure 7. Temperature profiles in the snow and ice of the M&U model and the two-layer model at minimum and maximum surface temperatures, respectively. The upper boundary of the models is a harmonic variation of the surface temperature with period 365 days and amplitude 10 K.

mass balance and heat exchange. Although the contribution from snow-covered thick ice is of secondary importance, it is still significant because of its large area percentage.

[47] Neglecting the oceanic heat flux alters the condition of ice formation at the bottom of the sea ice, in addition to changing the temperature gradient in the ice slab. Instead of melting, ice formation is taking place underneath thick floes as well, now dominating the total mass balance. Increased ice production also enlarges the ice mass transfer from thin to thick ice classes, resulting in a greater ice thickness in the classes >40 cm in the sensitivity run. Despite the large increase in ice production, the heat exchange is only slightly reduced. The increase of the area-weighted net heat flux under thick ice is due to its increased percentage in area.

[48] The reduction of the net heat flux due to the presence of a snow cover changes the thermodynamic ice growth at the bottom of the thick floes by the same amount as does the presence of an oceanic heat flux. However, while the oceanic heat flux affects both thick and thin ice, and has almost no influence on the net heat transfer from ocean to atmosphere, neglect of the snow cover on thick floes changes the overall energy balance dramatically.

[49] *Eicken et al.* [1994] estimated, based on data from different expeditions, that up to 50% of the sea ice in the Weddell Sea becomes flooded sometime throughout a winter period. The common notion that the formation of snow ice from snow slush in places where sea water infiltrated the lower snow layers is a relevant process within the ice mass budget, observed in situ by *Lytle et al.* [2000] in the East Antarctic region, is fully confirmed by our case study for the region west of Maud Rise. As the potential of bottom melting by high oceanic fluxes is larger here than in other regions of the Weddell Sea, the formation of snow ice effectively balances the impact of the large oceanic heat fluxes, that not only tend to cause bottom melting, but also to lower h_{fb}. The melting at the bottom is compensated by freezing at the top, leaving net ice formation to refreezing leads, with the overall result of reduced impact of oceanic fluxes on ice thickness. The heat exchange, however, is virtually uninfluenced.

[50] For the data set used in this study, each of the processes considered above contributes a significant amount to the energy and/or the ice mass balance. Compiling all results sheds light on the influence of the snow cover on the melting potential of the oceanic heat flux, which could be expressed in three stages: (1) Under cold winter conditions, the oceanic heat flux cannot compensate for the large conductive heat flux through snow-free ice, basically because of the almost linear temperature gradient between water and air temperature. (2) Snow precipitation, expressed by the ratio h_s/h_i, primarily reduces the heat conduction in the ice slab, thus increasing the melting potential at the bottom of the sea ice. (3) Further accumulation of snow (increasing h_s) causes bottom melting (decreasing h_i) and eventually the flooding condition is reached. At this stage, bottom melting is compensated, or even overruled. Under the given conditions, our combined models are in stage 1 (for leads) and at the margin from stage 2 to stage 3 (consolidated floes). Stages 2 and 3 could also be of importance for the lifetime of a large polynya. Although polynya formation can be explained by purely dynamic events [*Holland*, 2001], its lifetime can be extended by a cyclonic thermal wind field, caused by intrusion of heat into the lower atmosphere [*Timmermann et al.*, 1999]. In this context, stage 2 of the sea ice-snow system could enhance polynya formation and maintenance, whereas stage 3 would reduce likely conditions for a persistent polynya. The seasonal and regional variability of snowfall, recently thoroughly reviewed by *Massom et al.* [2001], will thus be an important factor for polynya formation and related processes.

[51] Despite the extensive data acquisition around ANZFLUX, a lack of adequate measurements still causes problems in interpreting our results. Fully instrumented, expensive buoys are normally placed at a sufficient distance from the floe edges on solid ice floes to prevent loss by floe collisions. It may be argued that their single point data therefore do not represent mean conditions for the class of older, snow-covered ice. On the other hand, buoys are deployed on ice floes typical in size and thickness for the region, thus minimizing the effect of floe-by-floe variability. During a few experiments, snow and ice thicknesses have been measured on the 1-m scale on individual floes, but this is not possible over periods of weeks and months to obtain temporal changes.

6. Conclusions

[52] Changes of ice thickness distribution, vertical temperature profiles, and energy fluxes associated with processes occurring during the development of a sea ice cover were studied for the period of 31 July to 16 September 1994, in the region of repeated occurrence of the Weddell Sea Polynya in the seventies. Data from drifting buoys [*Kottmeier et al.*, 1997] deployed during the ANZFLUX experiment in 1994 [*McPhee et al.*, 1996] provided means of forcing and validating process related models with in situ data. A consistent physical and empirical representation of the sea ice processes results from this effort. Being closely related to observed data, this integrated approach permits the sensitivity of sea ice development to be studied under stringent boundary conditions, in contrast to large-scale sea ice models [*Hibler and Ackley*, 1983; *Harder and Lemke*, 1994], where boundary conditions are less well known. Atmospheric forcing in large-scale sea ice models, for example, is usually specified by numerical model calculation (NMC) analyses. As they tend to smooth wind and temperature distributions, they are also likely to be biased in certain regions [*Kottmeier et al.*, 1997] and specify ocean heat fluxes by a constant basin-wide estimate; the sea ice cover is described without continuous adjustment to observables.

[53] Certain implications for large-scale sea ice modeling result from this work. It is shown that the temperature distribution and related thermal properties of snow-covered sea ice can be represented by a one-dimensional thermodynamic sea ice model, on condition that measured atmospheric forcing data and actual snow depth, as well as oceanic heat fluxes are available, and flooding and snow ice formation processes are taken into account in a simplified form. Under these circumstances, the comparison with buoy-measured temperature profiles in snow and ice shows that the model yields reasonable results. An event of sea ice flooding, for instance, occurring in mid-August, is evident in changes of the measured temperature distribution, and is also successfully reproduced by the model. In some large-

scale models, the effects of snow and formation of snow ice are already accounted for, also resulting in significant effects on longer timescales [*Fichefet and Maqueda*, 1999; *Wu et al.*, 1999].

[54] Twin runs with a one-dimensional two-layer model, which neglects heat storage, and the more complex one-dimensional model, without snow ice formation, indicate that mean heat fluxes in the upper sea ice and snow show insignificant discrepancies when averaged over several weeks. The surface temperature and infrared emission, especially, differ by less than 0.1% on average over the 47 days modeling period. Larger differences on shorter timescales lead to definite overestimation of ablation at the bottom of the ice in the two-layer model. The results imply that the simple linear vertical temperature distributions in two-layer thermodynamic models, widely used in large-scale sea ice models, are only suitable for considering temporally averaged heat fluxes at the surface, but are weaker when considering mass balances and instantaneous quantities.

[55] The sensitivity of sea ice formation to snow cover, being the limiting factor for heat exchange, emphasizes the importance of considering the thickness distribution and types of sea ice. Despite the relative small area occupied by snow-free, refreezing leads, they contribute a significant amount to the net heat flux and ice production. Although sea ice thickness plays a minor role for the direct heat loss to the atmosphere as soon as a thin snow cover is present, it is the key quantity for the mass balance, linking the impact of oceanic heat fluxes and snow ice formation caused by flooding.

[56] To conclude, all processes occurring during sea ice growth, related to snow cover, oceanic heat flux, and refreezing of leads, are crucial for the development of a sea ice covered region in the eastern Weddell Sea west of Maud Rise. Neglecting just one component of the system results in a significant change of the related energy and mass balances.

[57] **Acknowledgments.** When doing the last changes on the manuscript, the authors living in Germany received the tragic news of Karoline Frey's accidental death in an Alaskan mountain range. We are deeply moved by the fate of this young woman at an age of 26. She impressed her friends and colleagues with her personal spirit, her enthusiasm for the polar regions, and her outstanding scientific talents. The authors are grateful to E. Andreas, S. F. Ackley, and M. McPhee for the data supplied on atmospheric properties and heat fluxes. The ECMWF data were contributed by the German Weather Service, Offenbach. SSM/I data were provided by the National Snow and Ice Data Center, University of Colorado, Boulder, Colorado, USA. Special thanks go to G. A. Maykut, who helped with numerical problems, and to Jörg Hartmann, who developed graphics packages, and provided useful advice on its use. We acknowledge the comments of Hajo Eicken and Doug Martinson as well as of two anonymous reviewers, which clearly helped to improve the analysis.

References

Assur, A., Composition of sea ice and its tensile strength, in *Arctic Sea Ice*, vol. 598, pp. 106–138, Natl. Res. Counc., U.S. Natl. Acad. Sci., Washington, D. C., 1958.

Beckmann, A., R. Timmermann, A. F. Pereira, and C. Mohn, The effect of flow at Maud Rise on the sea-ice cover: Numerical experiments, *Ocean Dyn.*, *52*, 11–25, 2001.

Cox, G., and W. Weeks, Brine drainage and initial salt entrapment in sodium chloride salt, *CRREL Res. Rep. 345*, pp. 1–46, Cold Reg. Res. and Eng. Lab., Hanover, N.H., 1975.

Cox, G., and W. Weeks, Numerical simulations of the profile properties of undeformed first-year sea ice during the growth season, *J. Geophys. Res.*, *93*, 12,449–12,460, 1988.

Eicken, H., Salinity profiles of Antarctic sea ice, field data and model results, *J. Geophys. Res.*, *97*, 15,545–15,557, 1992.

Eicken, H., M. A. Lange, H.-W. Hubberten, and P. Wadhams, Characteristics and distribution patterns of snow and meteoric ice in the Weddell Sea and their contribution to the mass balance of sea ice, *Ann. Geophys.*, *12*, 80–93, 1994.

Eicken, H., H. Fischer, and P. Lemke, Effects of the snow cover on Antarctic sea ice and potential modulation of its response to climate change, *Ann. Glaciol.*, *21*, 369–376, 1995.

Eisen, O., and C. Kottmeier, On the importance of leads in sea ice to the energy balance and ice formation in the Weddell Sea, *J. Geophys. Res.*, *105*, 14,045–14,060, 2000.

Fichefet, T., and M. M. Maqueda, Modelling the influence of snow accumulation and snow-ice formation on the seasonal cycle of the antarctic sea-ice cover, *Clim. Dyn.*, *15*, 251–268, 1999.

Frey, K., Datenanalyse und Modellierung der Wärmeleitung im polaren Meereis, Master's thesis, Inst. fur Meteorologie und Klimaforschung, Karlsruhe, Germany, 1999.

Gloersen, P., W. J. Campbell, D. J. Cavalieri, J. C. Comiso, C. L. Parkinson, and H. J. Zwally, Arctic and Antarctic sea ice: 1978–1987, *NASA Spec. Publ., SP-511*, 1992.

Golden, K., S. Ackley, and V. Lytle, The percolation phase transition in sea ice, *Science*, *282*, 2238–2241, 1998.

Gordon, A. L., Seasonality of southern ocean sea ice, *J. Geophys. Res.*, *86*, 4193–4197, 1981.

Gordon, A. L., C. Chen, and W. Metcalf, Winter mixed layer entrainment of Weddell deep water, *J. Geophys. Res.*, *89*, 637–640, 1984.

Grenfell, T. C., and G. A. Maykut, The optical properties of ice and snow in the Arctic basin, *J. Glaciol.*, *18*, 445–463, 1977.

Harder, M., and P. Lemke, Modelling the extent of sea ice ridging in the Weddell Sea, in *Polar Oceans and Their Role in Shaping the Global Environment*, *Geophys. Monogr. Ser.*, vol. 85, edited by O. M. Johannessen, R. D. Muench, and J. E. Overland, pp. 187–197, AGU, Washington, D. C., 1994.

Hibler, W. D., III, and S. F. Ackley, Numerical Simulation of the Weddell Sea Pack Ice, *J. Geophys. Res.*, *88*, 2873–2887, 1983.

Holland, D. M., Explaining the Weddell polynya–A large ocean eddy sched at Maud Rise, *Science*, *292*, 1697–1700, 2001.

Jeffries, M. O., S. Li, R. A. Jana, H. R. Krouse, and B. Hurst-Cushing, Late winter first-year ice floe thickness variability, seawater flooding and snow ice formation in the Amundsen and Ross Seas, in *Antarctic Sea Ice: Physical Processes*, *Interactions and Variability*, *Antarct. Res. Ser.*, vol. 74, edited by M. O. Jeffries, pp. 69–87, AGU, Washington, D. C., 1998.

Kondo, J., Air-sea bulk transfer coefficients in diabatic conditions, *Boundary Layer Meteorol.*, *9*, 91–112, 1975.

König-Langlo, G., and E. Augstein, Parameterization of the downward long-wave radiation at the Earth's surface in polar regions, *Meteorol. Z.*, *3*, 343–347, 1994.

Kottmeier, C., and L. Sellmann, Atmospheric and oceanic forcing of Weddell sea ice motion, *J. Geophys. Res.*, *101*, 20,809–20,824, 1996.

Kottmeier, C., et al., Wind, temperature and ice motion statistics in the Weddell Sea, report, Int. Programme for Antarct. Buoys, World Clim. Res. Programme, Geneva, 1997.

Lange, M. A., and H. Eicken, The sea ice thickness distribution in the northwestern Weddell Sea, *J. Geophys. Res.*, *96*, 4821–4837, 1991.

Launiainen, J., and B. Cheng, Modelling of ice thermodynamics in natural water bodies, *Cold Reg. Sci. Technol.*, *27*, 153–178, 1998.

Lemke, P. A., A coupled one-dimensional sea ice-Ocean model, *J. Geophys. Res.*, *92*, 13,164–13,172, 1987.

Lytle, V. I., R. Massom, N. Bindoff, A. Worby, and I. Allison, Wintertime heat flux to the underside of east Antarctic pack ice, *J. Geophys. Res.*, *105*, 28,759–28,769, 2000.

Maksym, T., and M. O. Jeffries, A one-dimensional percolation model of flooding and snow ice formation on antarctic sea ice, *J. Geophys. Res.*, *105*, 26,313–26,331, 2000.

Martinson, D. G., Evolution of the Southern Ocean winter mixed layer and sea ice; open ocean water formation and ventilation, *J. Geophys. Res.*, *95*, 11,641–11,654, 1990.

Martinson, D. G., Antarctic ocean-ice interaction: Implications from ocean bulk property distributions, in *Antarctic Sea Ice: Physical Processes*, *Interactions and Variability*, *Antarct. Res. Ser.*, vol. 74, edited by M. J. Jeffries, pp. 243–271, AGU, Washington, D. C., 1998.

Martinson, D. G., P. D. Killworth, and A. L. Gordon, A convective model of the Weddell polynya, *J. Phys. Oceanogr.*, *11*, 466–487, 1981.

Massom, R., et al., Snow on Antarctic sea ice, *Rev. Geophys.*, *39*, 413–445, 2001.

Maykut, G. A., Energy exchange over young sea ice in the central Arctic, *J. Geophys. Res.*, *83*, 3646–3658, 1978.

Maykut, G. A., Large-scale heat exchange and ice production in the central Arctic, *J. Geophys. Res.*, *87*, 7971–7984, 1982.

Maykut, G. A., and N. Untersteiner, Numerical predictions of the thermodynamic response of arctic sea ice to environmental changes, *RM-5003-PR*, Rand Corp., Santa Monica, Calif., 1969.

Maykut, G. A., and N. Untersteiner, Some results from a time-dependent thermodynamic model of sea ice, *J. Geophys. Res.*, *76*, 1550–1575, 1971.

McPhee, M. G., S. F. Ackley, P. Guest, B. A. Huber, D. G. Martinson, J. H. Morison, R. D. Muench, L. Padman, and T. P. Stanton, The Antarctic Zone Flux Experiment, *Bull. Am. Meteorol. Soc.*, *77*, 1221–1232, 1996.

McPhee, M. G., C. Kottmeier, and J. H. Morison, Ocean heat flux in the central Weddell Sea during winter, *J. Phys. Oceanogr.*, *29*, 1166–1179, 1999.

Muench, R. D., J. H. Morison, L. Padman, D. Martinson, P. Schlosser, B. Huber, and R. Hohmann, Maud Rise revisited, *J. Geophys. Res.*, *106*, 2423–2440, 2001.

Parkinson, C. L., On the development and cause of the Weddell polynya in a sea ice simulation, *J. Phys. Oceanogr.*, *13*, 501–511, 1983.

Rapley, M., and V. Lytle, Brine infiltration in the snow cover of sea ice in the eastern Weddell Sea, Antarctica, *Ann. Glaciol.*, *27*, 461–465, 1998.

Semtner, A. J., Jr., A model for the thermodynamic growth of sea ice in numerical investigations of climate, *J. Phys. Oceanogr.*, *6*, 379–389, 1976.

Shine, K. P., and A. Henderson-Sellers, The sensitivity of a thermodynamic sea ice model to changes, *J. Geophys. Res.*, *90*, 2243–2250, 1985.

Smith, S. D., R. D. Muench, and C. H. Pease, Polynyas and leads: An overview of physical processes and environment, *J. Geophys. Res.*, *95*, 9461–9475, 1990.

Sturm, M., J. Holmgren, M. König, and K. Morris, The thermal conductivity of seasonal snow, *J. Glaciol.*, *43*, 26–41, 1997.

Timmermann, R., P. Lemke, and C. Kottmeier, Formation and maintainance of a polynya in the Weddell Sea, *J. Phys. Oceanogr.*, *29*, 1251–1264, 1999.

Untersteiner, N., On the mass and heat budget of Arctic sea ice, *Arch. Meteorol. Geophys. Bioklimatol.*, *12*, 151–182, 1961.

Worby, A. P., M. O. Jeffries, W. F. Weeks, K. Morris, and R. Jaña, The thickness distribution of sea ice and snow cover during late winter in the Bellinghausen and Amundsen Seas, Antarctica, *J. Geophys. Res.*, *101*, 28,441–28,455, 1996.

Wu, X., F. Budd, V. Lytle, and R. Massom, Effects of snow on Antarctic sea ice simulations in a coupled atmosphere-sea ice model, *Clim. Dyn.*, *15*, 127–143, 1999.

Zwally, H. J., J. C. Comiso, C. L. Parkinson, W. J. Campbell, F. D. Carsey, and P. Gloersen, Antartic sea ice: 1973–1976, *NASA Spec. Publ.*, *459*, 1983.

O. Eisen, Alfred-Wegener-Institut für Polar- und Meeresforschung, Columbusstr., 27515 Bremerhaven, Germany. (oeisen@awi-bremerhaven.de)

M. Hasel, Institut für Meteorologie und Klimaforschung, Universität Karlsruhe, Kaiserstr. 12, 76133 Karlsruhe, Germany. (markus.hasel@imk.fzk.de)

C. Kottmeier, Institut für Meteorologie und Klimaforschung, Universität Karlsruhe/Forschungszentrum Karlsruhe, Kaiserstr. 12, 76133 Karlsruhe, Germany. (kottmeier@imk.physik.uni-karlsruhe.de)